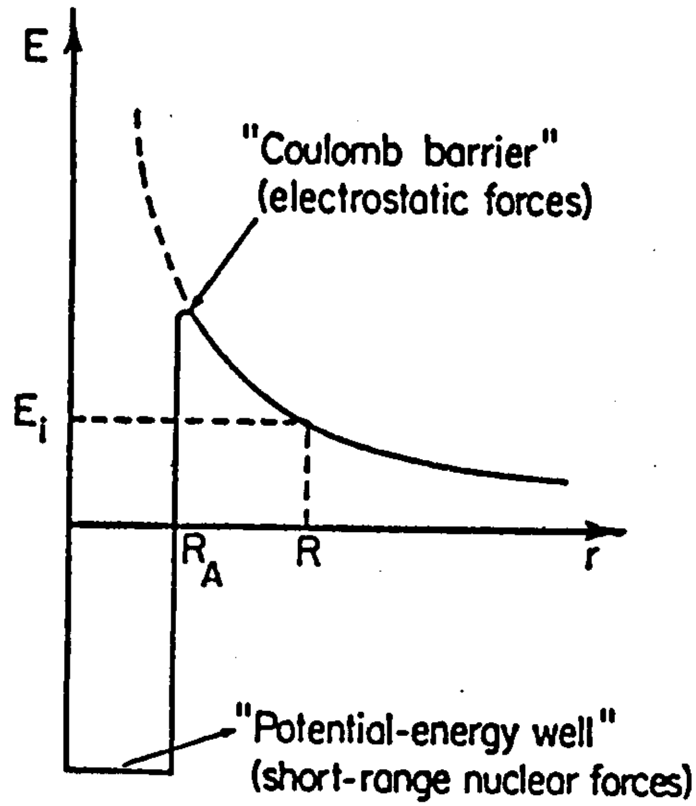

Fig. 6.1. Potential energy E as a function of the distance r from the nuc
R_A is the nuclear radius.

$$P = \exp\left[-\frac{4\pi}{h}\sqrt{(2m)}\int_{R_A}^{R}\sqrt{(U(r) - E_i)}\,dr\right]$$

where h is Planck's constant, m is the reduced mass of the alpha par

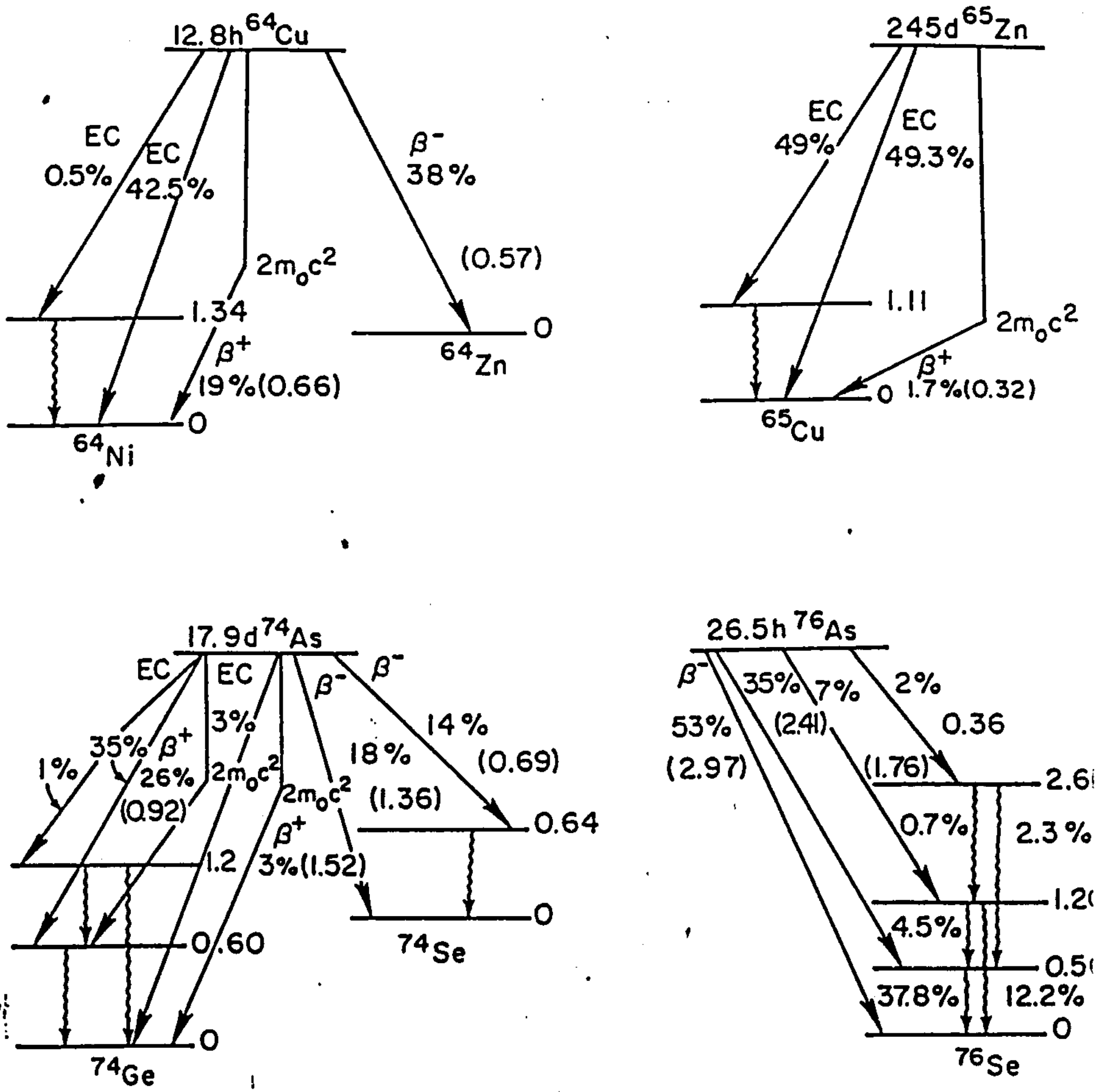

Figure 4.2 Decay schemes of some nuclides with complex modes of disintegration Quantitative measurement of these radionuclides may be made by selecting the type and energy of a particular radiation and correcting the disintegration rate for the fraction of decays by that radiation.

6.1a

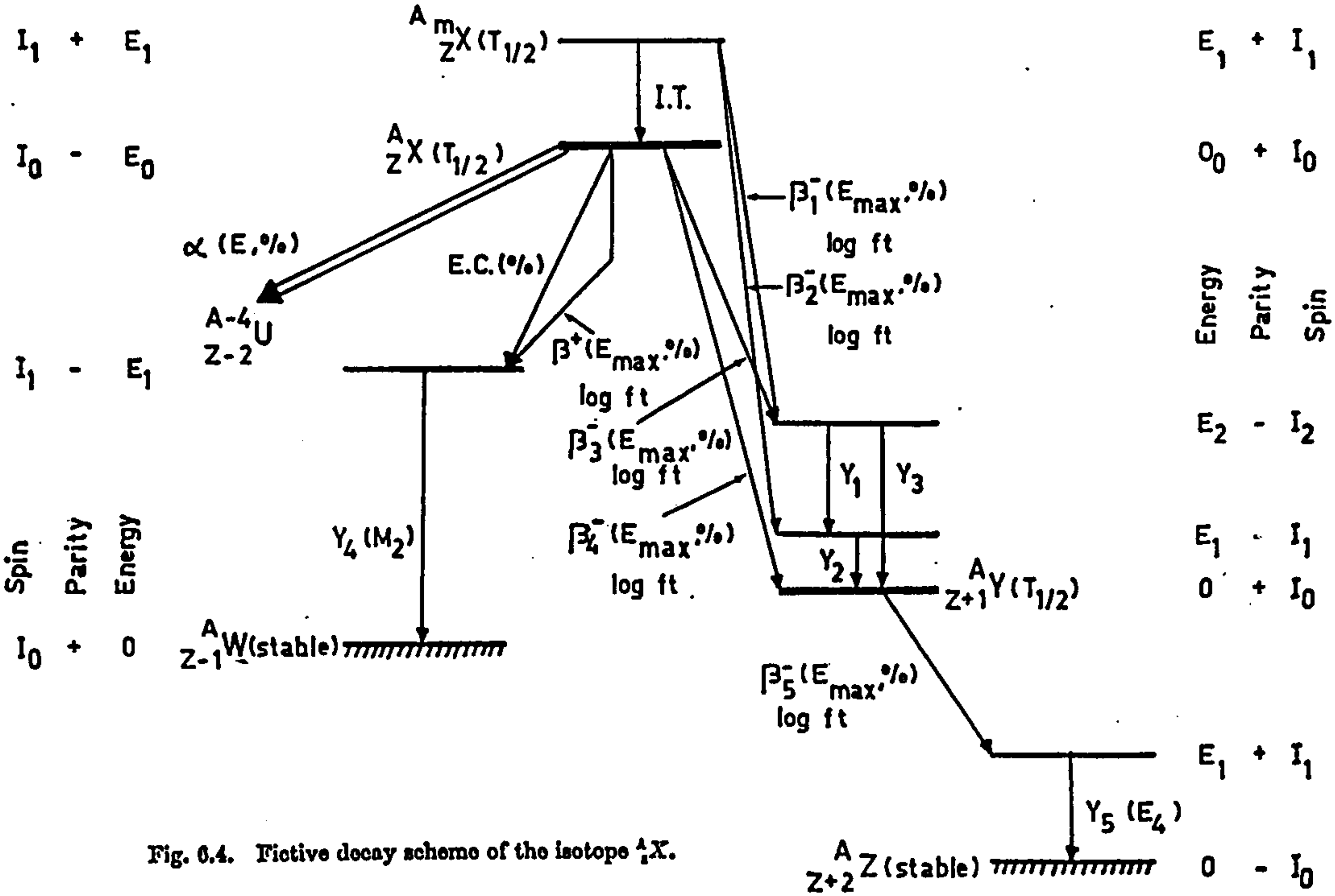

Fig. 6.4. Fictive decay scheme of the isotope $^A_Z X$.

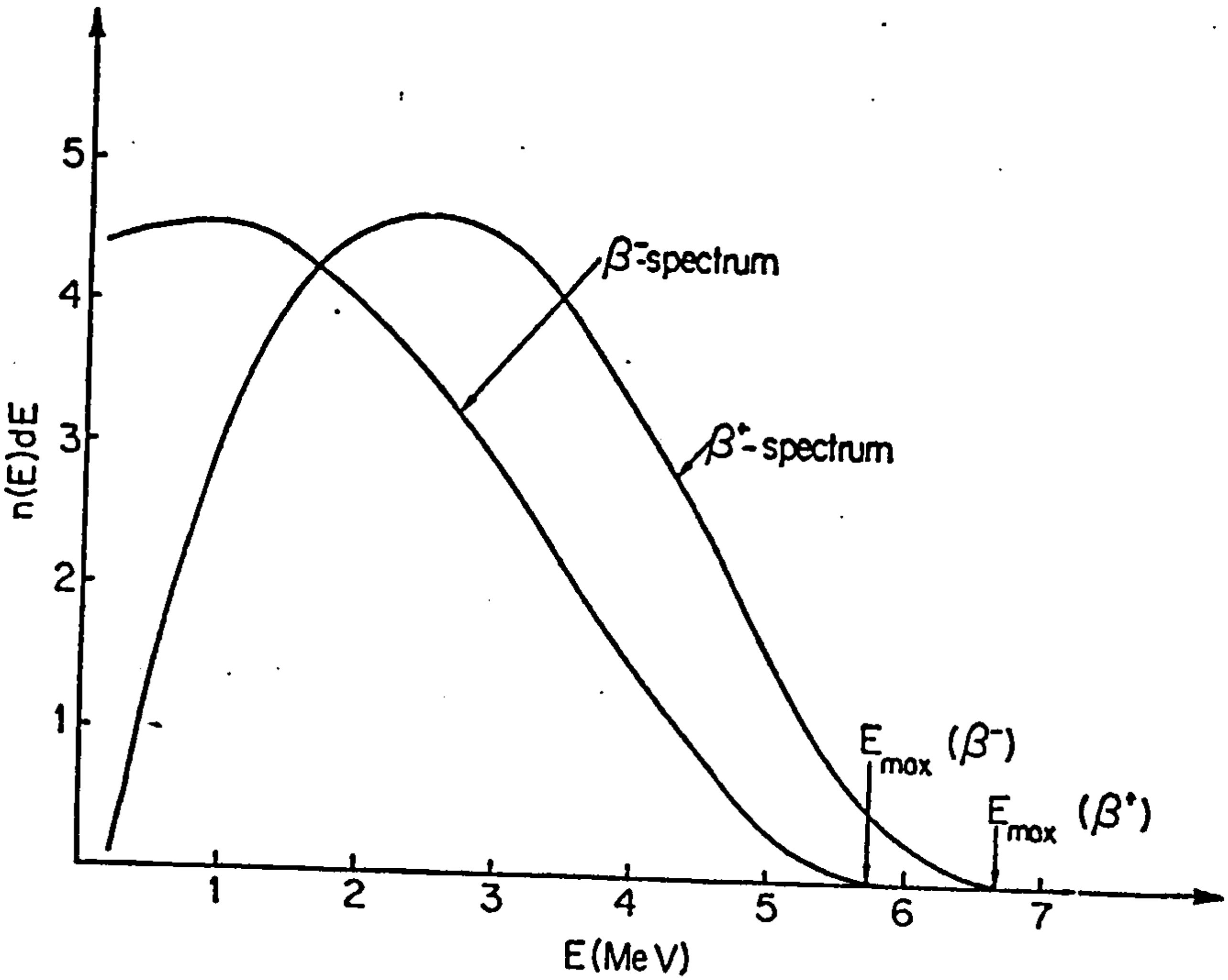

Fig. 6.2. Electron and positron spectrum of the isotope ^{64}Cu (6).

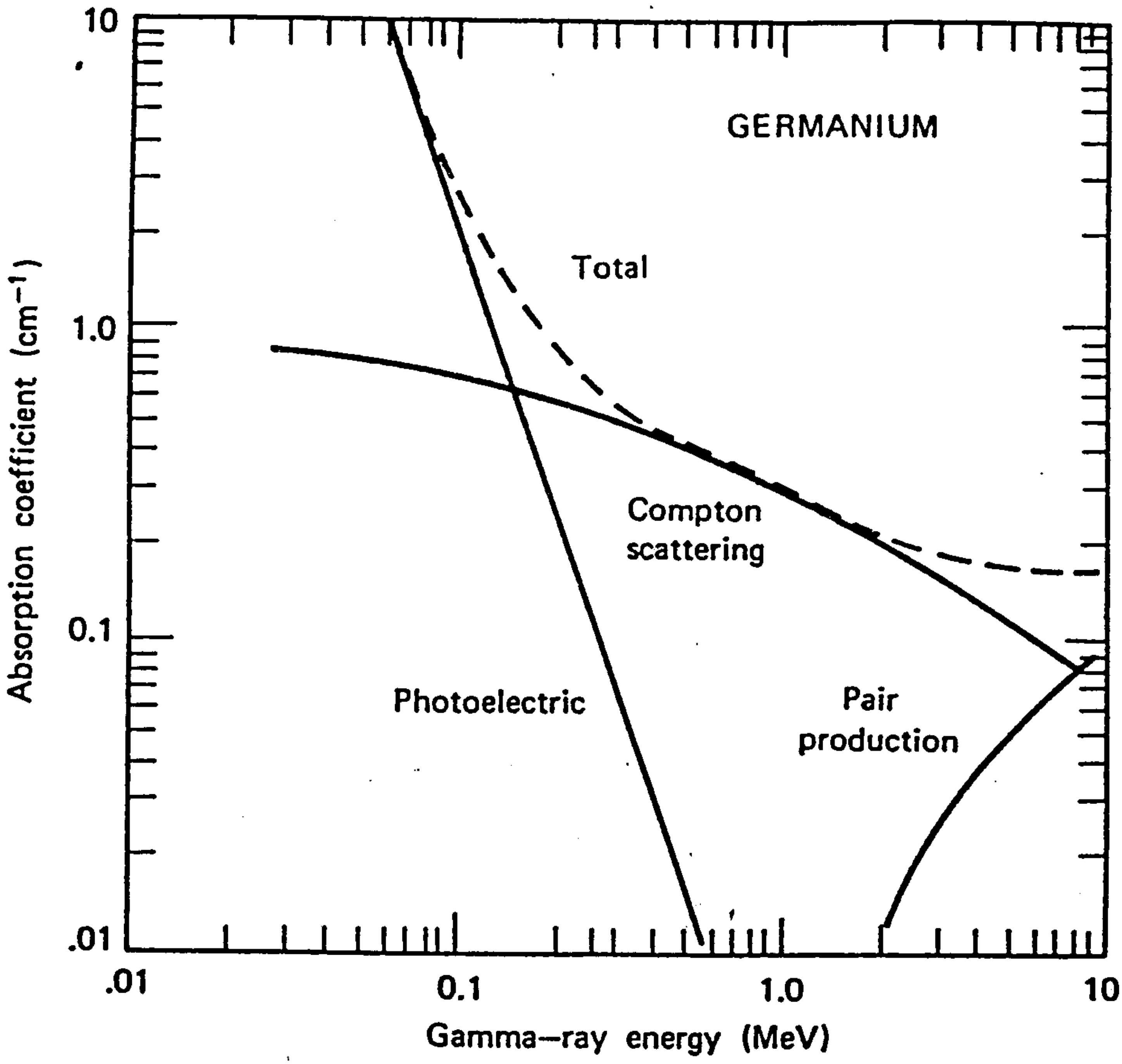

Figure 6.20 Partial and total absorption coefficients for gamma rays in germanium. [From G. Dearnaley and D. C. Northrop, *Semiconductor Counters for Nuclear Radiations* (Wiley, New York, 1966), p. 16.]

6.2c

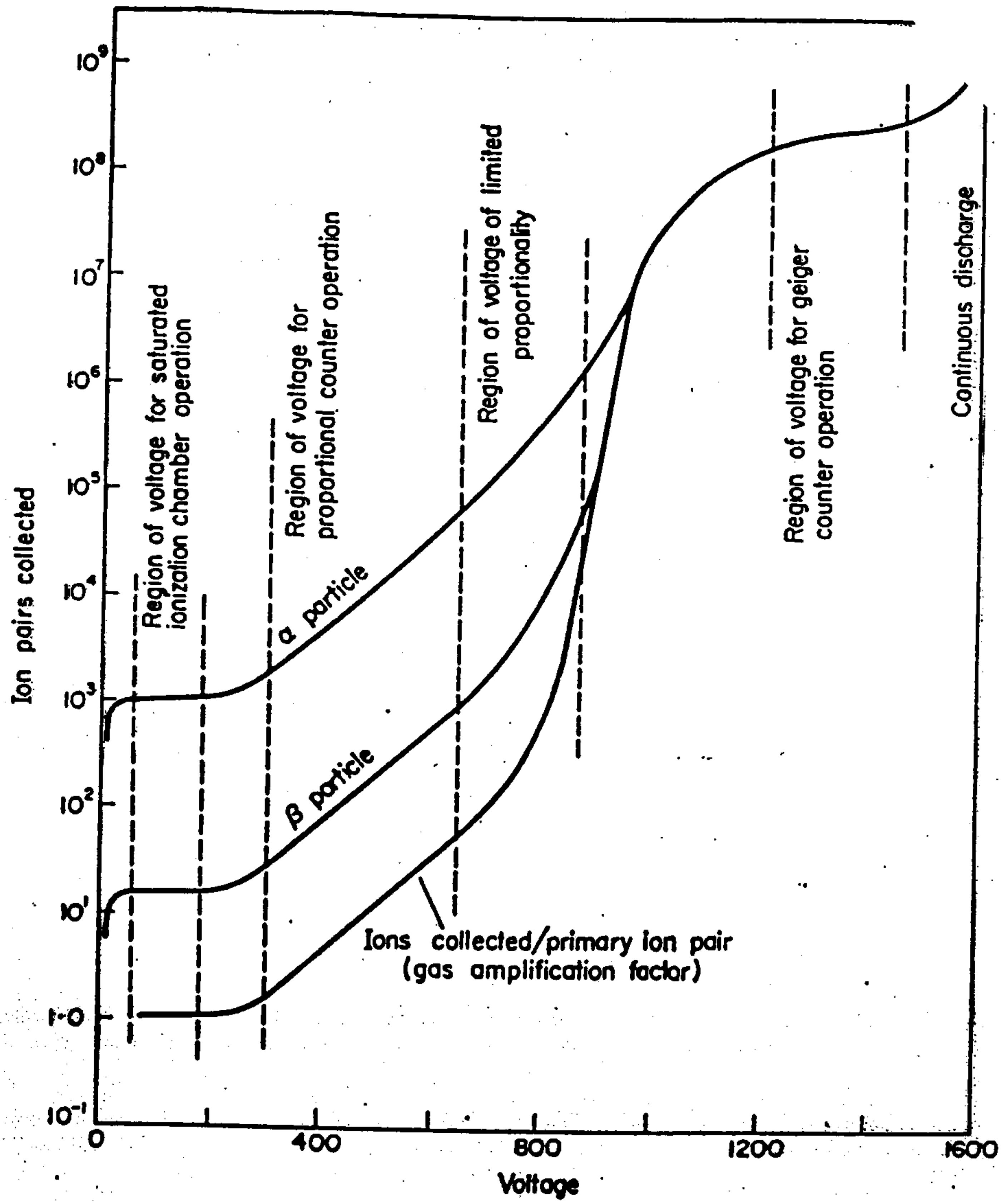

IG. 2.10 Characteristics of an idealized counter as a function of voltage

6.3a

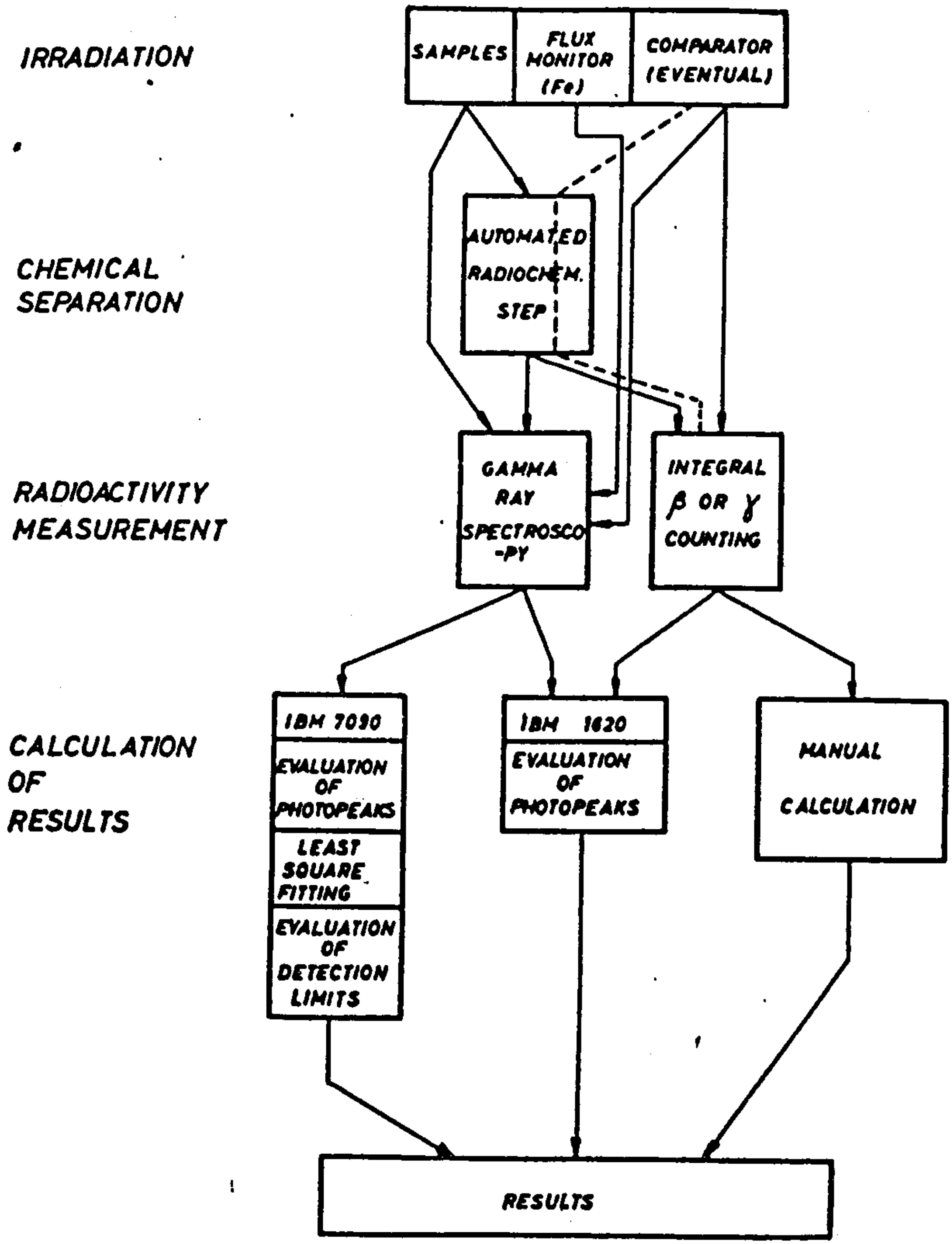

Figure 7.6 A flow sheet for an automated activation analysis system which includes radiochemical separations to concentrate the desired radionuclides or remove interfering radionuclides. [From F. Girardi, G. Guzzi, J. Pauly, and R. Pietra, The Use of an Automated System Including a Radiochemical Step in

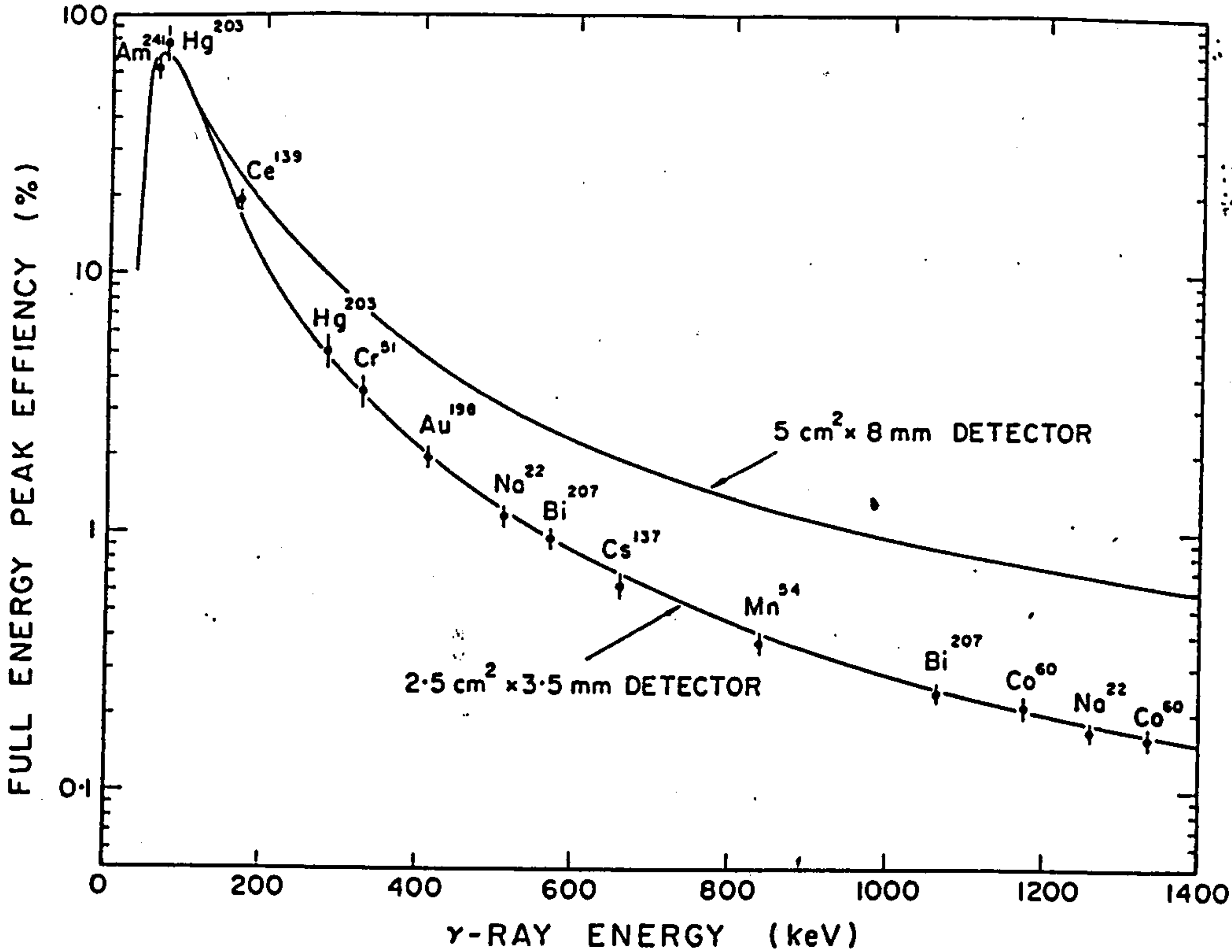

Figure 6.22 Full-energy peak efficiencies for two sizes of Ge(Li) detectors. At 1 MeV the efficiency of about 1% for the larger detector is almost four times that of the smaller detector. [From G. T. Ewan and A. J. Tavendale, High-resolution Studies of γ-Ray Spectra Using Li-Drift Germanium γ-Ray Spectrometers, *Can. J. Phys.* 42, 2286 (1964).]

6.3d

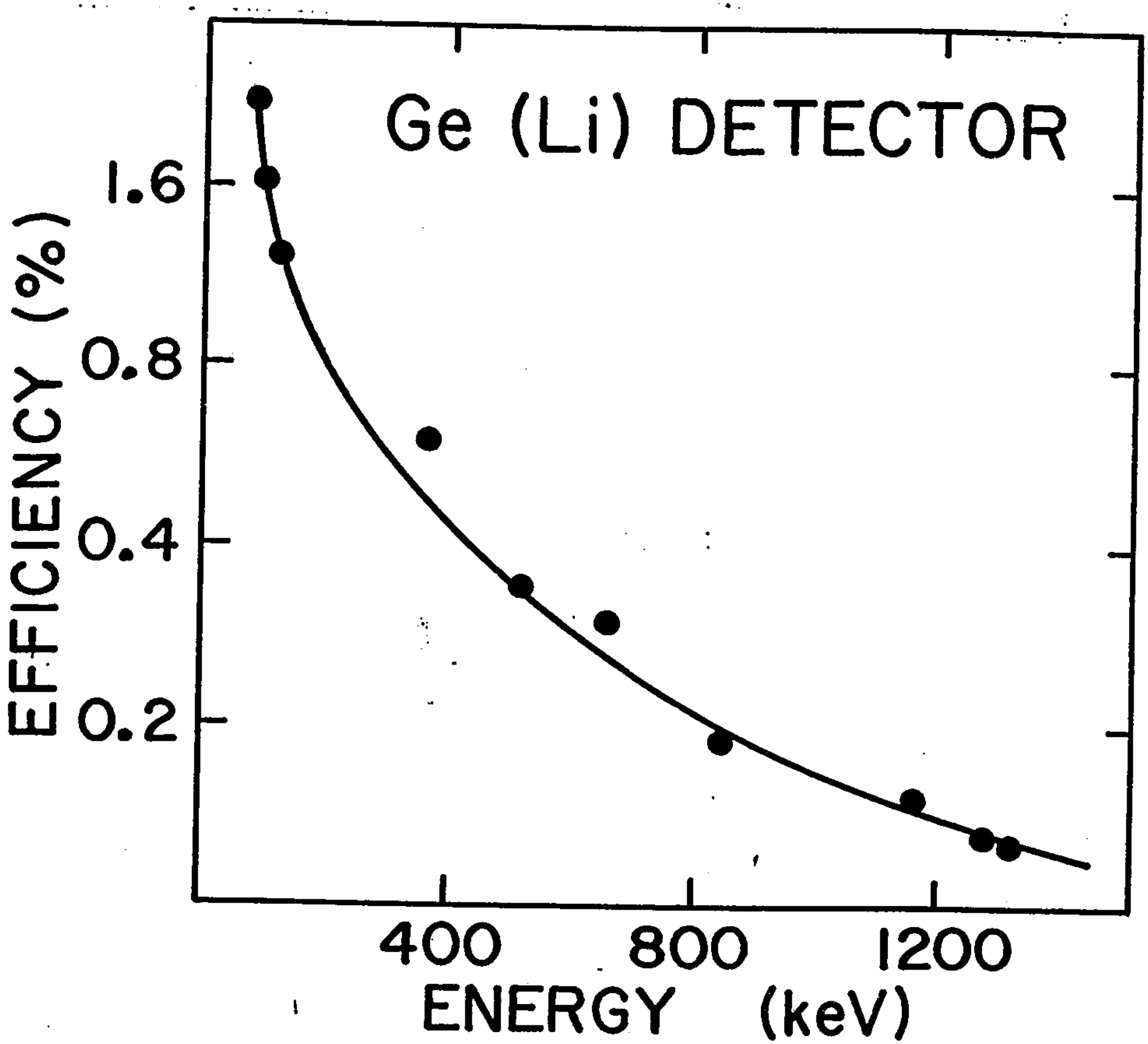

FULL-ENERGY PEAK EFFICIENCIES OF A Ge(Li) detector

6.3d

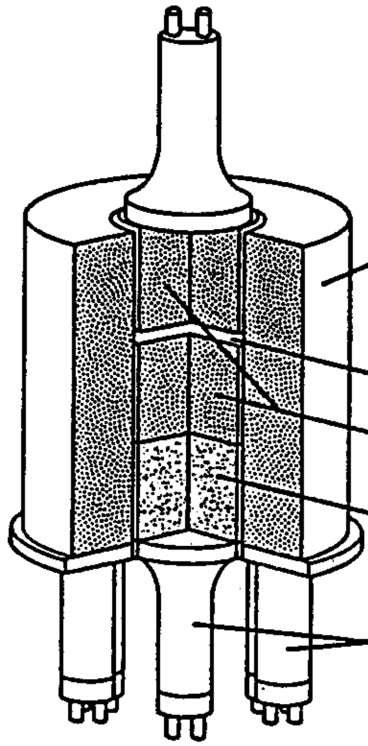

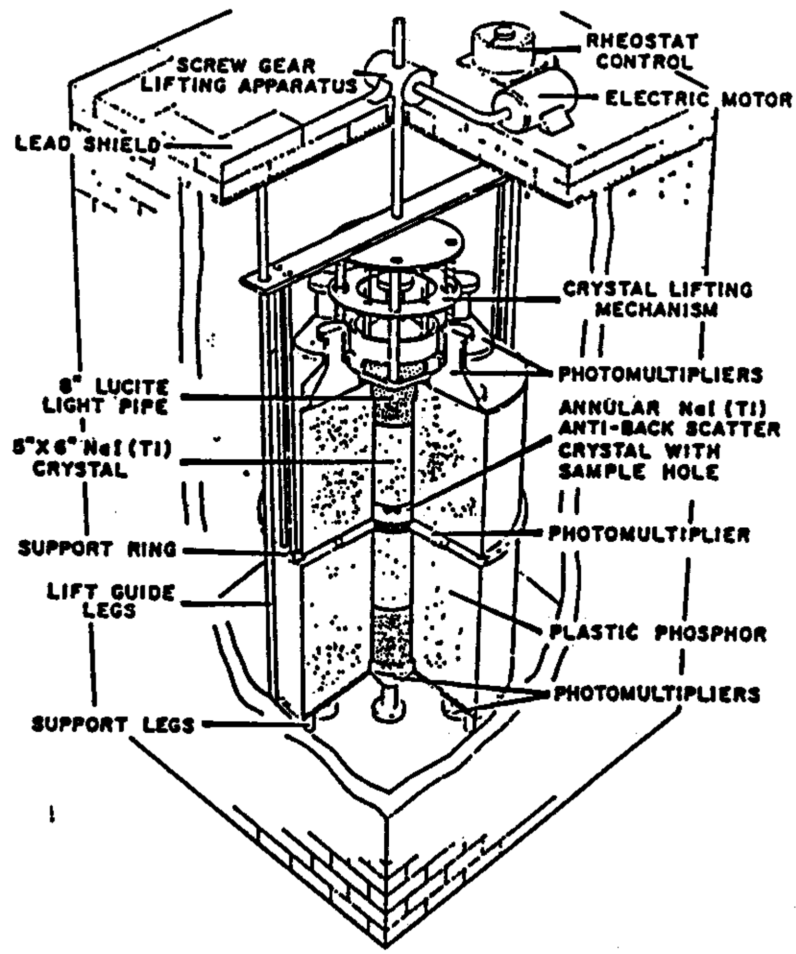

Figure 8.8 Cut-away views of a 2-NaI(Tl)-phosphor shield detector system for multidimensional gamma-ray spectrometry. [From R. W. Perkins and D. E. Robertson, in *Modern Trends in Activation Analysis* (Texas A&M University, College Station, 1965), pp. 48–57].

6.3e

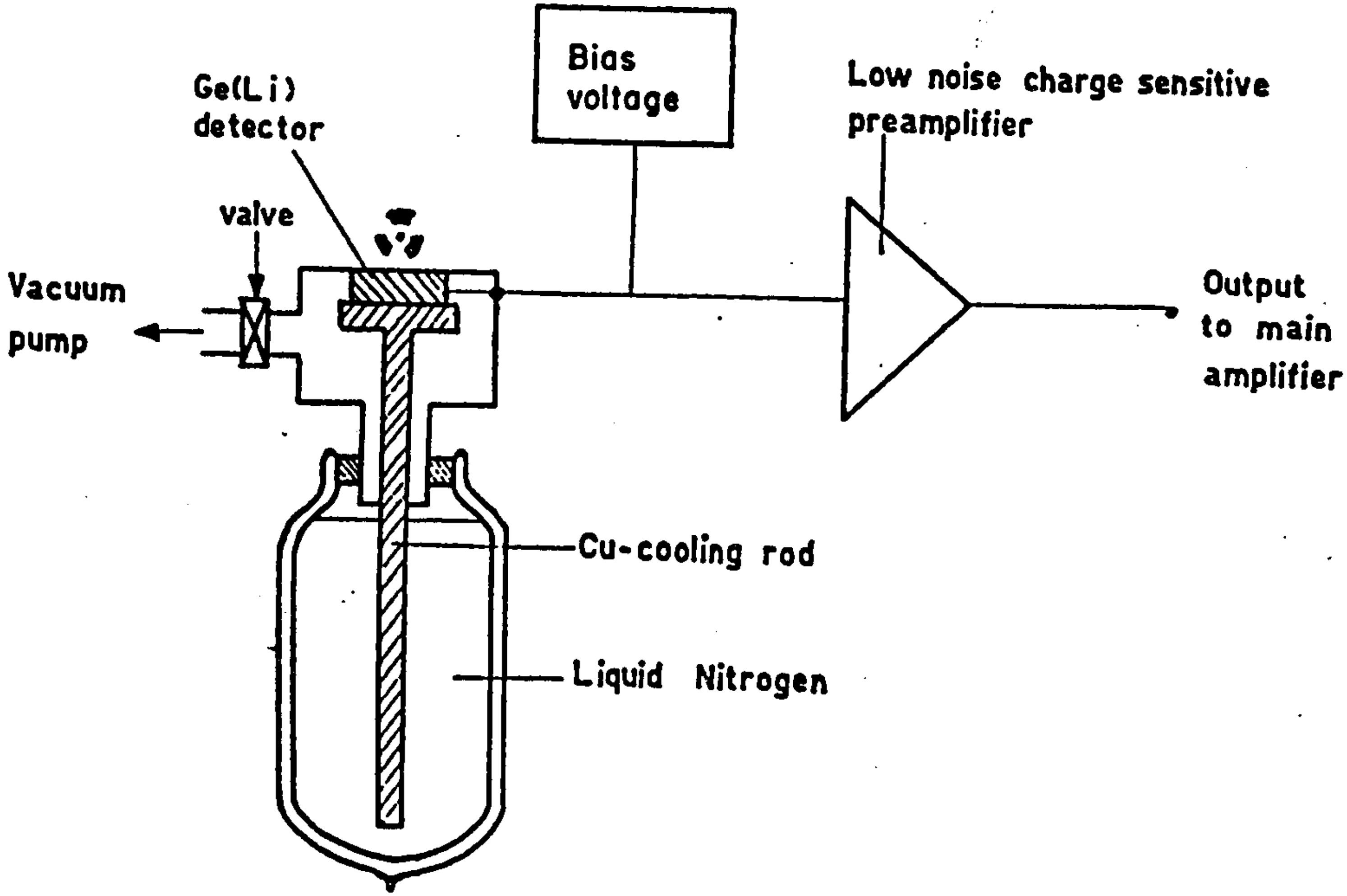

Fig. 6.23. Scheme of a typical Ge(Li) detector mounting.

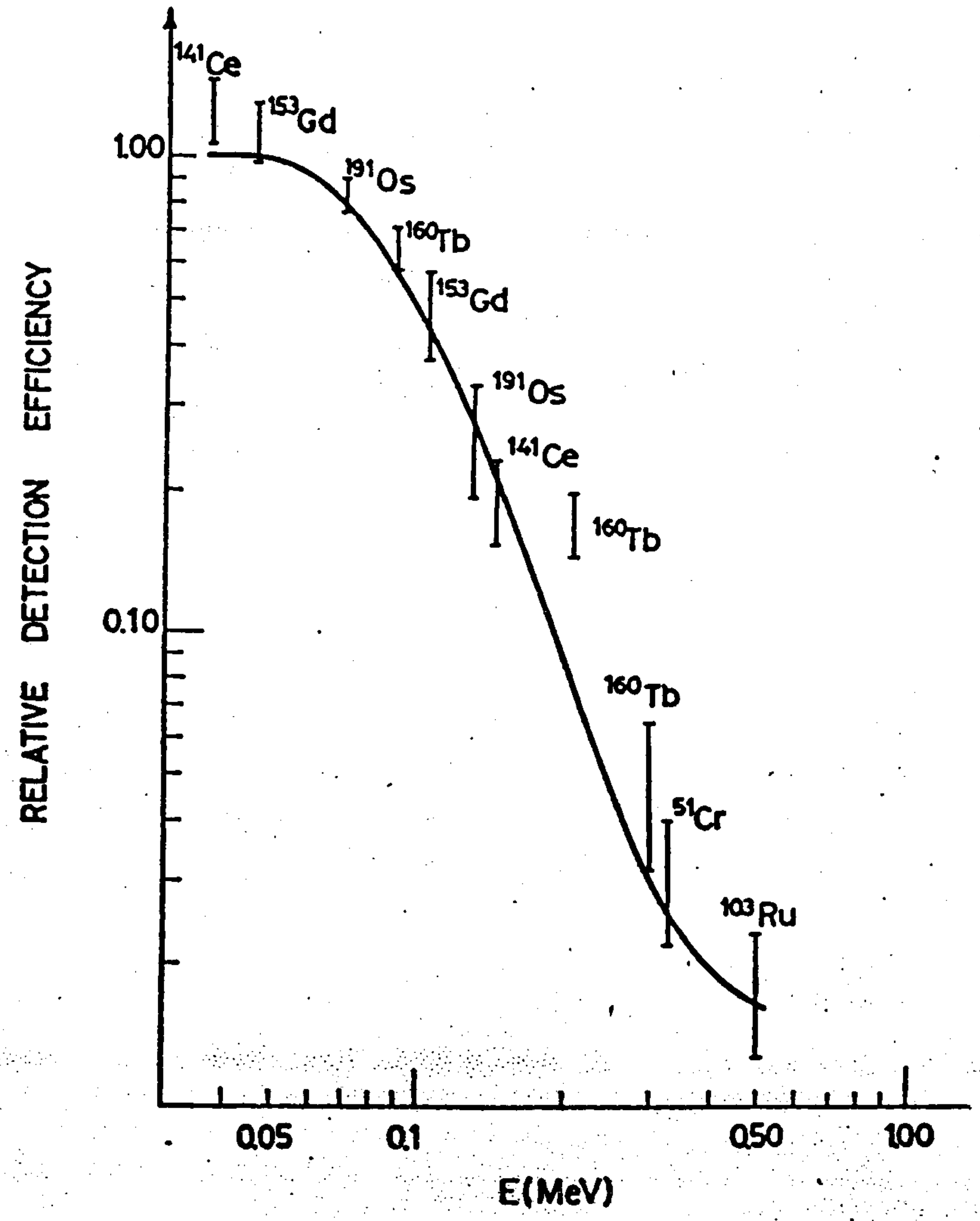

Fig. 6.25. Calculated photopeak detection efficiency ratio for a wafer of 7.5 cm diameter × 0.1 cm thickness, provided with a 37

6.3d

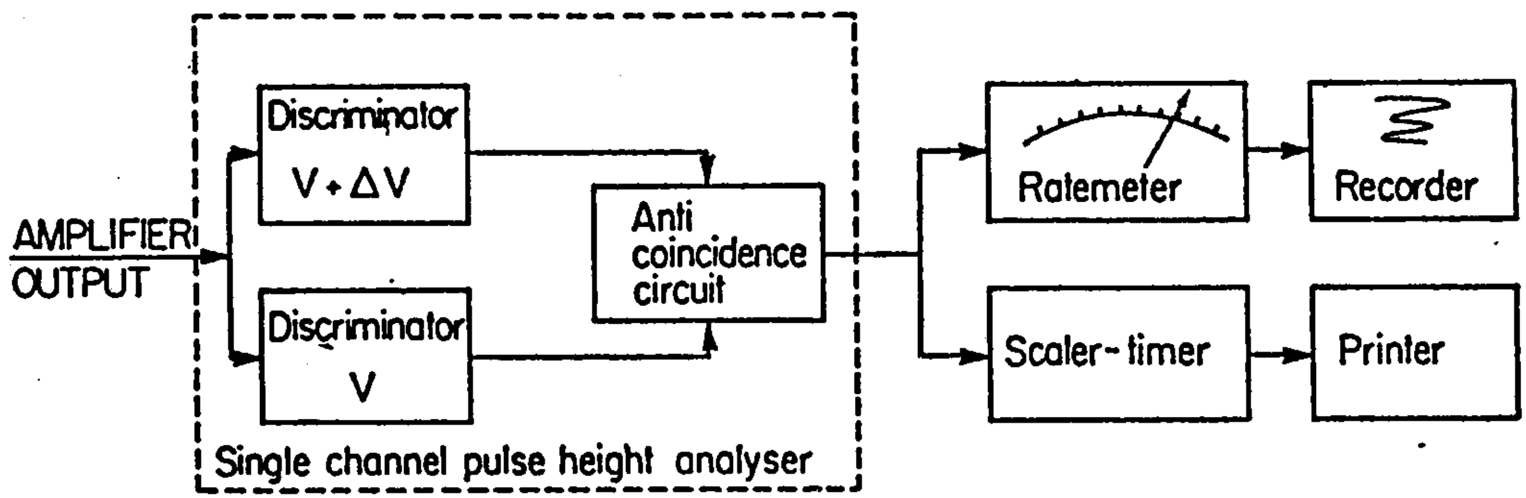

Fig. 6.26. Scheme of a single channel analyzer and related equipment.

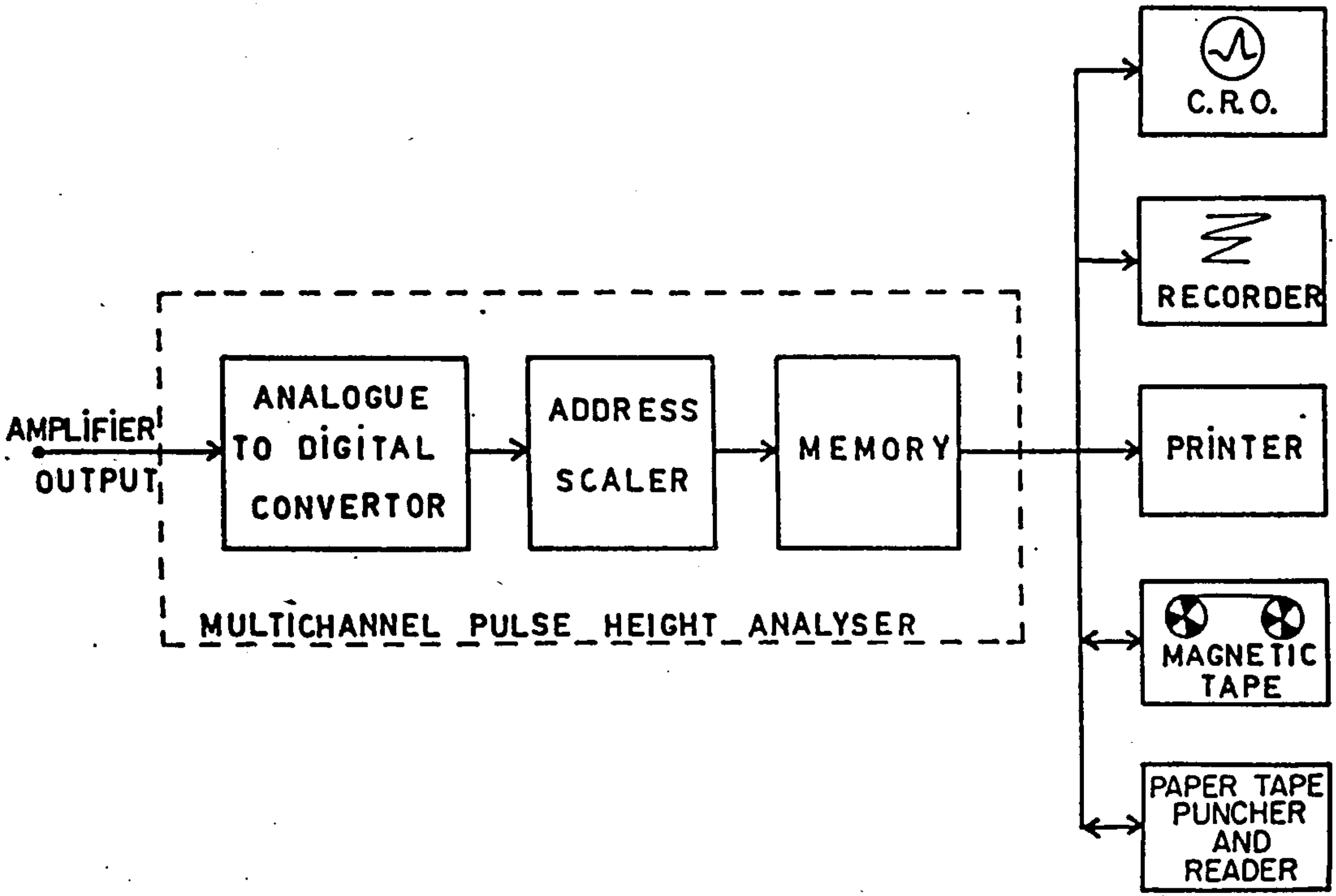

Fig. 6.27. Scheme of a multichannel analyzer and related equipment.

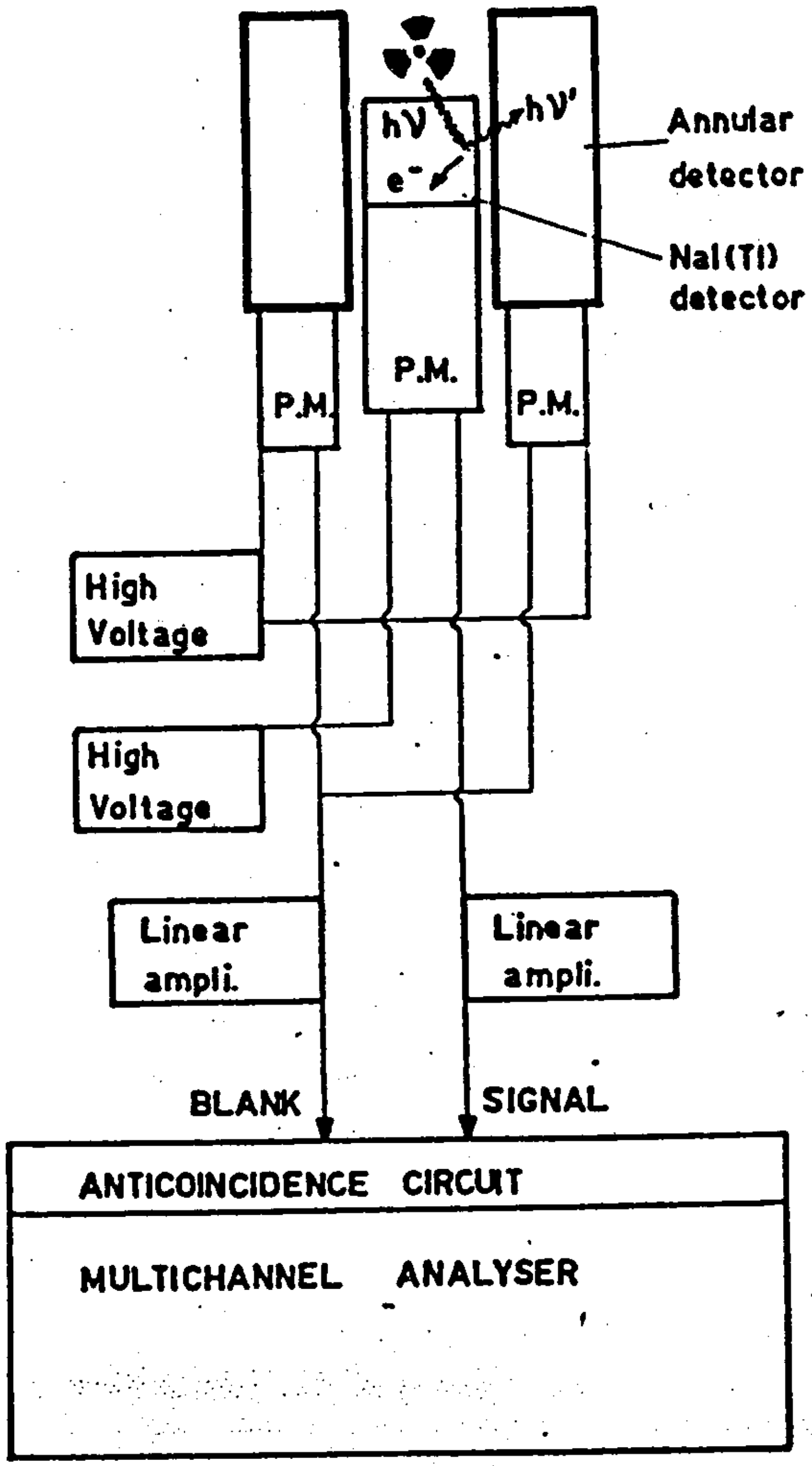

Fig. 6.36. Principle diagram of a Compton suppression spectrometer: an annular detector in anticoincidence.

6.3e

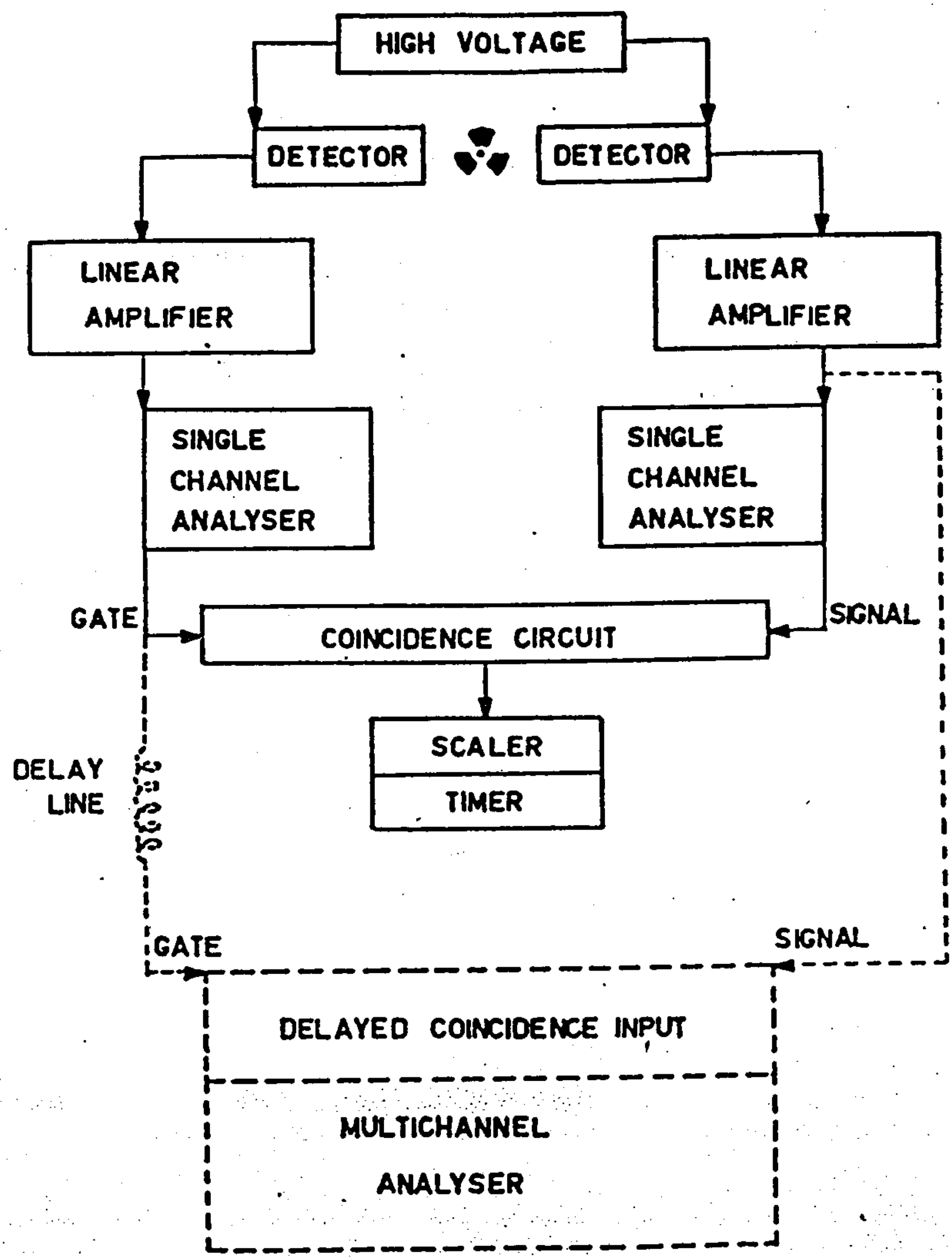

Fig. 6.32. Principle diagram of a "slow" coincidence spectrometer.

6.32

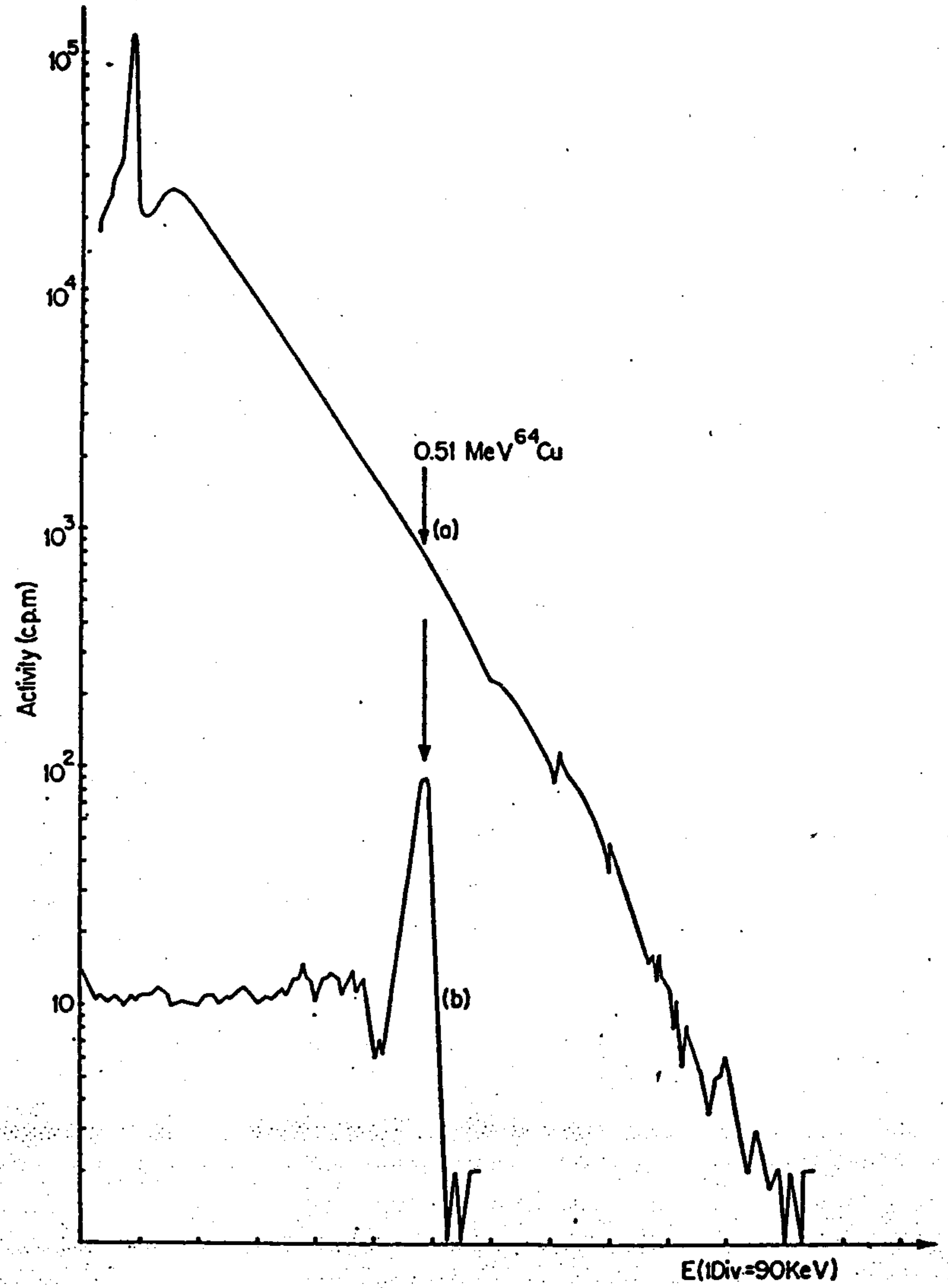

Fig. 6.34. Gamma spectrum of the ^{64}Cu annihilation radiation with the Bremsstrahlung spectrum of ^{210}Bi, measured without (a) and with (b) a coincidence technique in a neutron irradiated 1 g Bi sample, containing 0.226 ppm Cu (84).